

## Interpreting single turnover catalysis measurements with constrained mean dwell times

Maicol A. Ochoa, Xiaochun Zhou, Peng Chen, and Roger F. Loring

Citation: *J. Chem. Phys.* **135**, 174509 (2011); doi: 10.1063/1.3657855

View online: <http://dx.doi.org/10.1063/1.3657855>

View Table of Contents: <http://jcp.aip.org/resource/1/JCPSA6/v135/i17>

Published by the [American Institute of Physics](#).

---

### Related Articles

Coverage effects in the adsorption of H<sub>2</sub> on Pd(100) studied by ab initio molecular dynamics simulations  
*J. Chem. Phys.* **135**, 174707 (2011)

Kinetic description of finite-wall catalysis for monatomic molecular recombination  
*Phys. Fluids* **23**, 117101 (2011)

Communication: Quantitative Fourier-transform infrared data for competitive loading of small cages during all-vapor instantaneous formation of gas-hydrate aerosols  
*J. Chem. Phys.* **135**, 141103 (2011)

Carbon dioxide adsorption in graphene sheets  
*AIP Advances* **1**, 032152 (2011)

On the formation of hydrogen gas on copper in anoxic water  
*J. Chem. Phys.* **135**, 084709 (2011)

---

### Additional information on *J. Chem. Phys.*

Journal Homepage: <http://jcp.aip.org/>

Journal Information: [http://jcp.aip.org/about/about\\_the\\_journal](http://jcp.aip.org/about/about_the_journal)

Top downloads: [http://jcp.aip.org/features/most\\_downloaded](http://jcp.aip.org/features/most_downloaded)

Information for Authors: <http://jcp.aip.org/authors>

### ADVERTISEMENT

**AIP**Advances

*Submit Now*

Explore AIP's new  
open-access journal

- Article-level metrics now available
- Join the conversation! Rate & comment on articles

## Interpreting single turnover catalysis measurements with constrained mean dwell times

Maicol A. Ochoa, Xiaochun Zhou, Peng Chen, and Roger F. Loring<sup>a)</sup>

*Department of Chemistry and Chemical Biology, Baker Laboratory, Cornell University, Ithaca, New York 14853, USA*

(Received 3 September 2011; accepted 14 October 2011; published online 7 November 2011)

Observation of a chemical transformation at the single-molecule level yields a detailed view of kinetic pathways contributing to the averaged results obtained in a bulk measurement. Studies of a fluorogenic reaction catalyzed by gold nanoparticles have revealed heterogeneous reaction dynamics for these catalysts. Measurements on single nanoparticles yield binary trajectories with stochastic transitions between a dark state in which no product molecules are adsorbed and a fluorescent state in which one product molecule is present. The mean dwell time in either state gives information corresponding to a bulk measurement. Quantifying fluctuations from mean kinetics requires identifying properties of the fluorescence trajectory that are selective in emphasizing certain dynamic processes according to their time scales. We propose the use of constrained mean dwell times, defined as the mean dwell time in a state with the constraint that the immediately preceding dwell time in the other state is, for example, less than a variable time. Calculations of constrained mean dwell times for a kinetic model with dynamic disorder demonstrate that these quantities reveal correlations among dynamic fluctuations at different active sites on a multisite catalyst. Constrained mean dwell times are determined from measurements of single nanoparticle catalysis. The results indicate that dynamical fluctuations at different active sites are correlated, and that especially rapid reaction events produce particularly slowly desorbing product molecules. © 2011 American Institute of Physics. [doi:10.1063/1.3657855]

### I. INTRODUCTION

Detection of molecular processes at the single-molecule level elucidates the nature and time scales of fluctuations not observable in a bulk measurement that averages over these processes. Single-molecule measurements of enzyme catalysis reveal these molecules to function as dynamic entities, interchanging among structures with different catalytic properties.<sup>1–22</sup> Chen and co-workers have identified a fluorogenic chemical reaction that is catalyzed by gold nanoparticles, which permits the investigation of this catalysis with single-turnover resolution.<sup>23–29</sup> The nanoparticles catalyze the solution phase reductive *N*-deoxygenation of a nonfluorescent reactant resazurin to a fluorescent product resorufin by hydroxylamine. Observation of fluorescence intensity over time from a single nanoparticle yields a binary trajectory showing transitions between a fluorescent state in which a single product molecule is adsorbed together with reactant molecules, and a nonfluorescent state in which no product molecules are adsorbed.<sup>23,25,26,28</sup> A fluorescent time period begins with the conversion of reactant to product, and terminates with desorption of the product. A nonfluorescent time period is initiated by desorption of the product and concludes with the conversion of reactant to product. Chen and co-workers have quantified the heterogeneity of reaction events<sup>23,25,26</sup> on these nanoparticles, have studied reactivity variations with nanoparticle size,<sup>28</sup> and have determined the

effects of dynamic surface restructuring<sup>23,28</sup> on the kinetics of catalysis and product desorption. Despite differences in the underlying chemistry and time scales, there is an important qualitative similarity between these nanoparticles and enzyme molecules. The protein molecule changes catalytic states through conformational transitions.<sup>18,19,30,31</sup> Active sites on the nanoparticle can change activity through dynamic restructuring of the metal surface, either as a spontaneous process or induced by the reaction of adsorbed molecules.<sup>32–35</sup> The two catalytic systems differ in that the nanoparticle has multiple active sites of potentially different types, that the number and types of site can vary from one particle to another, and that for one particle, the number and types of sites can vary in time. Thus, catalysis by nanoparticles raises issues that do not pertain to an enzyme with a single active site, such as the existence of static or dynamic correlations among reaction and desorption processes at different sites.

Fluorescence trajectories may be quantified by calculating distributions of dwell times in the fluorescent and nonfluorescent states.<sup>36</sup> For the simplifying case treated here of saturating reactant concentration, the first moment of the distribution of dwell times in the nonfluorescent state yields a time-averaged rate constant for the rate of the catalytic reaction for a particular nanoparticle. When averaged over trajectories from many different particles, the result is the reciprocal of the reaction rate constant as determined in a conventional experiment on a bulk solution with nanoparticles. Similarly the mean dwell time in the fluorescent state contains the same information as the bulk rate constant for the desorption of product molecules from the

<sup>a)</sup> Author to whom correspondence should be addressed. Electronic mail: roger.loring@cornell.edu.

nanoparticle surface. Determining the detailed microscopic dynamics associated with individual catalytic events requires constructing quantities whose information content goes beyond these simple averages, and whose properties permit the assessment of kinetic models that describe both mean dynamics and fluctuations from the mean.<sup>4,5,8,11–15,18,19,36–58</sup>

In this work we propose the use of *constrained mean dwell times* to analyze fluorescence trajectories from single nanoparticles. These are mean dwell times in one state subject to a constraint on the immediately preceding dwell time in the other state. For example, we define  $\bar{t}_{L<}(\tau_D)$  to be the averaged dwell time in the fluorescent (L, light) state given that the preceding dwell time in the nonfluorescent (D, dark) state does not exceed a specified time  $\tau_D$ . If there were no correlation between these two dwell times, then  $\bar{t}_{L<}(\tau_D)$  would equal the unconstrained mean dwell time in L,  $\bar{t}_L$ . This would be the case, for example, if the distribution of possible rate constants governing a particular product desorption event were uninfluenced by the value of the rate constant for the reaction that generated that product molecule. Even if such correlations exist, for sufficiently long  $\tau_D$ ,  $\bar{t}_{L<}(\tau_D)$  must approach  $\bar{t}_L$ , which gives only bulk information. If these rate constants are correlated over some finite time scale, then at sufficiently short values of  $\tau_D$ , the mean is *selective* as it only includes fluorescent periods preceded by especially short nonfluorescent periods. If, for example, an active site at which desorption is unusually slow is also one in which reaction is especially rapid, then for the subset of events that contribute to  $\bar{t}_{L<}(\tau_D)$  for small  $\tau_D$  the mean dwell time in L will be longer than  $\bar{t}_L$ . In this scenario,  $\bar{t}_{L<}(\tau_D)$  as a function of  $\tau_D$  will decay to  $\bar{t}_L$  from greater values. The time scale of this decay will reflect the rates of the slowest reaction processes, since once  $\tau_D$  exceeds these time scales, the constrained mean loses its selectivity and approaches the unconstrained mean. Conversely if sites with rapid desorption also tend to promote rapid reaction, then  $\bar{t}_{L<}(\tau_D)$  will rise from smaller values to an asymptotic value of  $\bar{t}_L$ . The qualitative appearance of a plot of  $\bar{t}_{L<}(\tau_D)$  versus  $\tau_D$  reveals correlations among reaction and desorption rates for sites characterized by disorder. The conjugate quantity  $\bar{t}_{L>}(\tau_D)$  is the mean time in the fluorescent state given that the preceding time in the nonfluorescent state is greater than  $\tau_D$ . For  $\tau_D = 0$ , this quantity equals the unconstrained mean  $\bar{t}_L$ , but it becomes more selective with increasing  $\tau_D$ . Depending upon the correlations among reaction and desorption rates,  $\bar{t}_{L>}(\tau_D)$ , either rises or decays to a nonzero asymptote as  $\tau_D \rightarrow \infty$ . Similar definitions yield constrained mean times in the nonfluorescent state,  $\bar{t}_{D<}(\tau_L)$  and  $\bar{t}_{D>}(\tau_L)$ , and these quantities may be qualitatively interpreted in analogous fashion.

Analyzing fluorescence trajectories from a catalyst with a single active site with constrained mean dwell times yields both qualitative and quantitative information about fluctuations from mean kinetics. We show here that these quantities are particularly well suited to probe correlations among reaction and desorption dynamics for catalysts with multiple active sites, such as nanoparticles or oligomeric enzymes. The constrained mean dwell times in L and D states are affected differently by the presence of multiple active sites. A particular dwell time in state D ends with the conversion of a reactant molecule to product, and the following dwell time in

L terminates with desorption of that same product molecule. Therefore,  $\bar{t}_{L<}(\tau_D)$  reflects correlations involving one reactant molecule and the product species produced by that molecule, even in the presence of multiple active sites. However, a particular dwell time in L ends with the desorption of a product molecule from one site, but the following dwell time in D ends with a chemical reaction that may be at the original site or may occur at a different site, making  $\bar{t}_{D<}(\tau_L)$  sensitive to system size in a different way from  $\bar{t}_{L<}(\tau_D)$ .

We employ the term *dynamic disorder* to refer to a rate process,<sup>59,60</sup> in which rate constants fluctuate in time among values governed by either a discrete<sup>4,7</sup> or a continuous<sup>11,13–15</sup> distribution. In Sec. II, we calculate constrained mean dwell times for a kinetic model with dynamic disorder analyzed by Yang and Cao<sup>5</sup> for single-molecule measurements of an enzyme with a single active site.<sup>15</sup> In this model, the unit of the active site plus adsorbate occupies discrete internal states, representing conformations for a protein or surface structures for a nanoparticle. The kinetics of conversion of the reactant and of desorption of product depend on these internal site states. The site states interconvert by a dynamic process, representing conformational transitions for the enzyme or surface reconstruction for the nanoparticle. In Sec. III, we generalize this model to an arbitrary number of active sites and consider the effects of spatial correlations among fluctuations in reactivity. In the model of *correlated fluctuations*, all active sites change state together, while in the model of *independent fluctuations*, the sites change states independently of each other. We demonstrate that the predictions of the constrained mean dwell times differ both qualitatively and quantitatively between the two models. We also describe a model of correlated domains of active sites that interpolates between these two limiting cases. In Sec. IV, we discuss constrained mean dwell times calculated from experimental fluorescence trajectories of single gold nanoparticles.<sup>23,28</sup> Our conclusions are summarized in Sec. V.

## II. SINGLE ACTIVE SITE

We first define a kinetic model for a catalyst with a single active site, and then generalize in Sec. III to models of a nanoparticle with  $N$  sites. The catalyst promotes the reaction of an adsorbed nonfluorescent reactant species denoted D to produce a fluorescent species L. The reactant concentration is taken to be sufficiently high that the rate of adsorption of the reactant to the unoccupied site is large compared to the rates of desorption of either reactant or product, so that the site may be assumed to be always occupied by either reactant or product. To anticipate the inhomogeneity of sites on a nanoparticle, we take the single site in the current model to have  $S$  internal states that may differ in catalytic activity and in desorption kinetics. These states interconvert through a dynamic process. Since there are  $S$  site states and the site can be occupied by either of two species, the system has  $2S$  possible states. States labeled  $D_1, \dots, D_S$  describe site occupation by the reactant, and states  $L_1, \dots, L_S$  represent site occupation by the product. The rate constant for conversion of reactant to product in site state  $\alpha$  is  $k_{D_\alpha}$  and the rate constant for desorption of species L is  $k_{L_\alpha}$ . Rates of interconversion among site states are taken

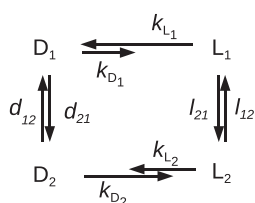


FIG. 1. Kinetic scheme for one active site with two states. State 2 has faster reaction and slower desorption of the product.

to depend on the identity of the species adsorbed at the site. The rate constant for transformation of site state  $\alpha$  to  $\gamma$  is  $d_{\gamma\alpha}$  ( $l_{\gamma\alpha}$ ) when the adsorbate is species D (L). The  $2S$ -dimensional vector of state probabilities evolves according to

$$|\dot{p}(t)\rangle = \mathbf{w}|p(t)\rangle, \quad (2.1)$$

$$\mathbf{w} = -\mathbf{w}_D - \mathbf{w}_L + \mathbf{w}_{DL} + \mathbf{w}_{LD}. \quad (2.2)$$

Here  $\mathbf{w}_D$  is nonzero only in the  $S$ -dimensional subspace of D states, with, e.g.,  $[w_D]_{D_\gamma, D_\gamma} = k_{D_\gamma} + \sum_{\alpha \neq \gamma} d_{\alpha\gamma}$  representing the total rate constant for probability loss from  $D_\gamma$  because of state changes and chemical reaction, and  $-[w_D]_{D_\alpha, D_\gamma} = d_{\alpha\gamma}$ , the interconversion rate constant from site state  $\gamma$  to  $\alpha$  when the site is occupied by a reactant. Similarly  $\mathbf{w}_L$  is nonzero only in the subspace of L states, with elements  $[w_L]_{L_\gamma, L_\gamma} = k_{L_\gamma} + \sum_{\alpha \neq \gamma} l_{\alpha\gamma}$  and  $[w_L]_{L_\alpha, L_\gamma} = -l_{\alpha\gamma}$ .  $\mathbf{w}_{LD}$  has nonzero elements  $[w_{LD}]_{L_\alpha, D_\alpha} = k_{D_\alpha}$ , the reaction rate constant for site state  $\alpha$ , and  $\mathbf{w}_{DL}$  has nonzero elements  $[w_{DL}]_{D_\alpha, L_\alpha} = k_{L_\alpha}$ , the rate constant for product desorption in site state  $\alpha$ . This kinetic scheme is shown in Fig. 1 for  $S = 2$ . If arrow length is taken to represent magnitude of rate constant, then this mechanism illustrates the case, discussed below in Sec. IV, in which the site state with more rapid reaction rate, state 2 in Fig. 1, has the slower product desorption rate. For subsequent analysis, it is convenient to define idempotent matrices  $\mathbf{s}_j$  with  $j = D, L$  that project into the subspaces of D and L states, respectively. For example, the only nonzero elements of  $\mathbf{s}_D$  are  $(\mathbf{s}_D)_{D_\alpha, D_\alpha} = 1$ . The components of the transition matrix in Eq. (2.2) may then be written as  $\mathbf{w}_D = \mathbf{s}_D \mathbf{w}_D$ ,  $\mathbf{w}_L = \mathbf{s}_L \mathbf{w}_L$ ,  $\mathbf{w}_{LD} = \mathbf{s}_L \mathbf{w}_D$ , and  $\mathbf{w}_{DL} = \mathbf{s}_D \mathbf{w}_L$ .

Equilibrium conditions for the spaces of D and L states are

$$\mathbf{w}_D |p\rangle = \mathbf{w}_{DL} |p\rangle, \quad (2.3)$$

$$\mathbf{w}_L |p\rangle = \mathbf{w}_{LD} |p\rangle, \quad (2.4)$$

with  $|p\rangle$  the  $2S$ -dimensional vector of probabilities in Eq. (2.1) at equilibrium. Probability conservation implies

$$\langle 1 | \mathbf{w}_{LD} = \langle 1 | \mathbf{w}_D, \quad (2.5)$$

$$\langle 1 | \mathbf{w}_{DL} = \langle 1 | \mathbf{w}_L. \quad (2.6)$$

Here,  $\langle 1 |$  indicates the  $2S$ -dimensional vector with elements  $\langle (1) |_{D_\alpha} = \langle (1) |_{L_\alpha} = 1$ . Combining these conditions connects equilibrium fluxes out of each state space,

$$\langle 1 | \mathbf{w}_{LD} |p\rangle = \langle 1 | \mathbf{w}_{DL} |p\rangle = \langle 1 | \mathbf{w}_L |p\rangle = \langle 1 | \mathbf{w}_D |p\rangle. \quad (2.7)$$

The latter pair of equalities follows from probability conservation associated with changes in site state.

A single molecule fluorescence study of this model system would yield a binary trajectory of fluorescent and nonfluorescent states. Fluorescence is observed in any of the states  $\{L_\alpha\}$ , and no fluorescence is produced when the state is one of  $\{D_\alpha\}$ . The dwell time  $t_L$  is the time elapsed between the onset of the fluorescent state and the succeeding transition to the nonfluorescent state, which corresponds to the time elapsed between conversion of reactant to product and desorption of the product. Similarly  $t_D$  is the time elapsed between desorption of the product and the next conversion of reactant to product. The equilibrium distribution of dwell times in D is defined by<sup>5</sup>

$$f_D(t_D) \equiv \frac{\langle 1 | \mathbf{w}_{LD} e^{-\mathbf{w}_D t_D} \mathbf{w}_{DL} |p\rangle}{\langle 1 | \mathbf{w}_{LD} |p\rangle}, \quad (2.8)$$

and is related to a simpler generating function  $g_D(t_D)$  by

$$f_D(t_D) = \frac{d^2 g_D(t_D)}{dt_D^2}, \quad (2.9)$$

$$g_D(t_D) \equiv \frac{\langle 1 | \mathbf{s}_D e^{-\mathbf{w}_D t_D} \mathbf{s}_D |p\rangle}{\langle 1 | \mathbf{w}_D |p\rangle}. \quad (2.10)$$

Equation (2.9) follows from differentiating Eq. (2.10) and applying Eqs. (2.3), (2.5), and (2.7). The mean dwell time in state D is the first moment of  $f_D(t_D)$ , given by

$$\bar{t}_D = \int_0^\infty dt_D t_D f_D(t_D) = g_D(0). \quad (2.11)$$

The distribution of dwell times in L,  $f_L(t_L)$ , is related to a generating function  $g_L(t_L)$  by the analogs of Eqs. (2.9) and (2.10) with  $D \leftrightarrow L$ .

In order to define constrained mean dwell times, these single-time distributions must be generalized to joint distributions for pairs of successive dwell times.<sup>5</sup> For example,  $f_{LD}(t_L, t_D)$  is defined<sup>5</sup> to be the joint probability distribution for an equilibrium system that a dark period of duration  $t_D$  is immediately followed by a fluorescent period of duration  $t_L$ ,

$$f_{LD}(t_L, t_D) \equiv \frac{\langle 1 | \mathbf{w}_{DL} e^{-\mathbf{w}_L t_L} \mathbf{w}_{LD} e^{-\mathbf{w}_D t_D} \mathbf{w}_{DL} |p\rangle}{\langle 1 | \mathbf{w}_{LD} |p\rangle}, \quad (2.12)$$

and is related to a generating function  $g_{LD}(t_L, t_D)$  by

$$f_{LD}(t_L, t_D) = \frac{\partial^2 g_{LD}(t_L, t_D)}{\partial t_D \partial t_L}, \quad (2.13)$$

$$g_{LD}(t_L, t_D) \equiv \frac{\langle 1 | \mathbf{s}_L e^{-\mathbf{w}_L t_L} \mathbf{w}_{LD} e^{-\mathbf{w}_D t_D} \mathbf{s}_D |p\rangle}{\langle 1 | \mathbf{w}_D |p\rangle}. \quad (2.14)$$

The corresponding distribution for  $t_L$  to be followed by  $t_D$ ,  $f_{DL}(t_D, t_L)$ , is obtained from Eqs. (2.12)–(2.14) with interchange of labels D and L. The constrained mean dwell time  $\bar{t}_{L <}(t_D)$  is defined to be the average dwell time in the fluorescent state L under the condition that the immediately preceding dwell time in the dark state D is less than a specified interval  $\tau_D$

$$\bar{t}_{L <}(\tau_D) \equiv \frac{\int_0^\infty dt_L t_L \int_0^{\tau_D} dt_D f_{LD}(t_L, t_D)}{\int_0^{\tau_D} dt_D f_D(t_D)}. \quad (2.15)$$

The denominator represents the total probability that a dwell time in D satisfies  $t_D < \tau_D$ . If successive dwell times in D and L are uncorrelated,  $f_{LD}(t_L, t_D) = f_L(t_L)f_D(t_D)$ , and  $\bar{t}_{L<}(\tau_D)$  equals the unconstrained mean  $\bar{t}_L$  as in Eq. (2.11) with  $D \rightarrow L$ . In the limit  $\tau_D \rightarrow \infty$ ,  $\bar{t}_{L<}(\tau_D)$  approaches  $\bar{t}_L$ . In the opposite limit  $\tau_D \rightarrow 0$ ,  $\bar{t}_{L<}(\tau_D)$  approaches a finite short-time value. This constrained mean dwell time may be expressed in terms of generating functions by performing the integral in the numerator of Eq. (2.15) using Eq. (2.13) and by evaluating the integral in the denominator of Eq. (2.15) using Eq. (2.9). Subtracting  $\bar{t}_L$  from this result yields the difference between constrained and unconstrained mean times,

$$\Delta\bar{t}_{L<}(\tau_D) \equiv \bar{t}_{L<}(\tau_D) - \bar{t}_L = \frac{-\bar{t}_L \dot{g}_D(\tau_D) - \int_0^\infty dt_L g_{LD}(t_L, \tau_D)}{1 + \dot{g}_D(\tau_D)}. \quad (2.16)$$

The information content of  $\Delta\bar{t}_{L<}(\tau_D)$  may be understood by evaluating Eq. (2.16) for  $S = 2$  in the limit of static disorder<sup>59–61</sup> in which site state interconversion rates  $d_{\alpha\gamma}$  and  $l_{\alpha\gamma}$  are much smaller than reaction rates  $k_{D\gamma}$  and product desorption rates  $k_{L\gamma}$ . In this limit, the matrices  $e^{-\mathbf{w}_D t_D}$  and  $e^{-\mathbf{w}_L t_L}$  are diagonal, and the generating functions  $g_D(t_D)$  in Eq. (2.10) and  $g_{LD}(t_L, t_D)$  in Eq. (2.14) are evaluated to give

$$\Delta\bar{t}_{L<}(\tau_D) = \left( \frac{p_{L_1} p_{L_2}}{\langle 1 | \mathbf{w}_L | p \rangle} \right) \times \left( \frac{(k_{L_1} - k_{L_2}) (e^{-k_{D_1} \tau_D} - e^{-k_{D_2} \tau_D})}{(1 - e^{-k_{D_1} \tau_D}) k_{D_1} p_{D_1} + (1 - e^{-k_{D_2} \tau_D}) k_{D_2} p_{D_2}} \right). \quad (2.17)$$

The derivation of this result relies on the static limit of Eq. (2.3) or (2.4),  $k_{D\gamma} p_{D\gamma} = k_{L\gamma} p_{L\gamma}$ . The equilibrium probabilities  $p_{L\gamma}$  and  $p_{D\gamma}$  in general depend on the rate constants for site state interconversion  $d_{\alpha\gamma}$  and  $l_{\alpha\gamma}$ , even in the limit in which they approach zero. The constrained mean dwell time difference in Eq. (2.17) approaches zero from either positive or negative values. Significant information can be deduced from its initial sign and from its asymptotic decay rate for long  $\tau_D$ . The initial algebraic sign is evident from Eq. (2.17) to be the sign of the product  $(k_{L_1} - k_{L_2})(k_{D_2} - k_{D_1})$ . Either the state with the larger reaction rate has the smaller product desorption rate as illustrated in Fig. 1, or the state with the larger reaction rate also has the larger desorption rate. For the case in which a particular state has the larger reaction rate but the smaller desorption rate,  $\Delta\bar{t}_{L<}(\tau_D) > 0$ . In this case, for small  $\tau_D$  the constrained mean time selects a subset of sites with rapid reaction and slow desorption. The mean time elapsed from reaction to desorption for this subensemble is longer than for the full ensemble, so that  $\bar{t}_{L<}(\tau_D) > \bar{t}_L$  and their difference is positive. For the case in which the state with the larger reaction rate also has the larger desorption rate,  $\bar{t}_{L<}(\tau_D)$  reflects a subensemble with rapid desorption. The mean time elapsed from reaction to desorption is short compared to that of the full ensemble, and  $\Delta\bar{t}_{L<}(\tau_D)$  approaches zero from negative values. The sign of  $\Delta\bar{t}_{L<}(\tau_D)$  indicates the correlation, if any, between reaction rate and desorption rate at a site.

The asymptotic decay rate of  $\Delta\bar{t}_{L<}(\tau_D)$  also carries useful information. For the case of well-separated rate constants for both reaction and desorption such that  $k_D^{\text{big}} \gg k_D^{\text{small}}$  and  $k_L^{\text{big}} \gg k_L^{\text{small}}$ ,  $\Delta\bar{t}_{L<}(\tau_D)$  in Eq. (2.17) approaches zero with decay constant  $k_D^{\text{small}}$ . For times less than or of order of  $(k_D^{\text{big}})^{-1}$ ,  $\bar{t}_{L<}(\tau_D)$  selects the subpopulation with a larger reaction rate, but for times comparable to or larger than  $(k_D^{\text{small}})^{-1}$ , this mean reflects the entire ensemble, and selectivity is lost. Thus, the rate constant for the slower of the two reaction processes may be extracted from the long  $\tau_D$  dependence of  $\Delta\bar{t}_{L<}(\tau_D)$ .

The complementary constrained mean time between reaction and desorption with the condition that the preceding elapsed time to reaction exceeds a certain value  $\tau_D$  is defined similarly to Eq. (2.15) as

$$\bar{t}_{L>}(\tau_D) \equiv \frac{\int_0^\infty dt_L t_L \int_{\tau_D}^\infty dt_D f_{LD}(t_L, t_D)}{\int_{\tau_D}^\infty dt_D f_D(t_D)}. \quad (2.18)$$

In the limit  $\tau_D \rightarrow 0$ ,  $\bar{t}_{L>}(\tau_D)$  approaches the unconstrained average  $\bar{t}_L$ , and in the opposite limit of  $\tau_D \rightarrow \infty$ , it approaches a finite asymptote. The difference between constrained and unconstrained mean times is

$$\Delta\bar{t}_{L>}(\tau_D) = \frac{-\bar{t}_L \dot{g}_D(\tau_D) - \int_0^\infty dt_L g_{LD}(t_L, \tau_D)}{\dot{g}_D(\tau_D)}. \quad (2.19)$$

This constrained time is readily interpreted for the  $S = 2$  static disorder case of Eq. (2.17),

$$\Delta\bar{t}_{L>}(\tau_D) = \left( \frac{p_{L_1} p_{L_2}}{\langle 1 | \mathbf{w}_L | p \rangle} \right) \times \left( \frac{(k_{L_2} - k_{L_1}) (e^{-k_{D_1} \tau_D} - e^{-k_{D_2} \tau_D})}{k_{D_1} e^{-k_{D_1} \tau_D} p_{D_1} + k_{D_2} e^{-k_{D_2} \tau_D} p_{D_2}} \right). \quad (2.20)$$

If site state 1 has the larger reaction rate  $k_{D_1} > k_{D_2}$ , then for  $\tau_D \geq (k_{D_1})^{-1}$ ,  $\Delta\bar{t}_{L>}(\tau_D)$  approaches a limit independent of  $\tau_D$  with the algebraic sign of  $k_{L_1} - k_{L_2}$ . If the site state with larger reaction rate also has the larger product desorption rate, then  $\Delta\bar{t}_{L>}(\tau_D)$  starts at zero at  $\tau_D = 0$  and increases to a positive asymptote. In this case, for large  $\tau_D$ ,  $\bar{t}_{L>}(\tau_D)$  reflects the subensemble with the smaller reaction rate and hence the smaller product desorption rate. This subensemble has a longer mean time to desorption than the full ensemble, so that  $\Delta\bar{t}_{L>}(\tau_D) > 0$ . The asymptote is approached for time scales comparable to the inverse of the larger reaction rate  $k_{D_1}$ . Thus the constrained time  $\Delta\bar{t}_{L<}(\tau_D)$  reaches its long  $\tau_D$  asymptote of zero with the smaller of the two reaction rates, and the complementary quantity  $\Delta\bar{t}_{L>}(\tau_D)$  reaches its nonzero asymptote at long  $\tau_D$  with the larger of the two reaction rates, providing distinct information. Conversely if the state with larger reaction rate has the smaller product desorption rate, then  $\Delta\bar{t}_{L>}(\tau_D)$  decays to a negative value as  $\tau_D$  increases, also with the larger reaction rate. Expressions for constrained time differences for the period between product desorption and subsequent reaction  $\Delta\bar{t}_{D<}(\tau_L)$  and  $\Delta\bar{t}_{D>}(\tau_L)$  can be obtained from the results just presented for  $\Delta\bar{t}_{L<}(\tau_D)$  and  $\Delta\bar{t}_{L>}(\tau_D)$  with interchange of labels  $L \leftrightarrow D$ .

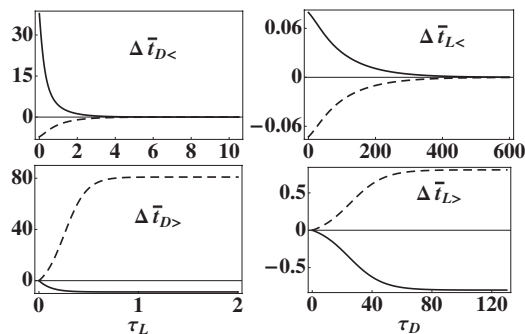


FIG. 2. Constrained mean dwell times are shown for a catalyst with one active site and two internal states. Differences between constrained and unconstrained mean times are plotted. Solid curves are calculated for reaction rate constants  $k_{D_1} = 0.1$  and  $k_{D_2} = 0.01$ , for product desorption rate constants  $k_{L_1} = 1$  and  $k_{L_2} = 10$ , and for site state changing rate constants  $d_{\alpha\gamma} = l_{\alpha\gamma} = 10^{-4}$ . Time unit is  $k_{L_1}^{-1}$ . Dashed curves are calculated for the same parameters, but with interchange of the values of  $k_{D_1}$  and  $k_{D_2}$ .

The characteristic appearances of plots of the four constrained mean times are shown in Fig. 2 for  $S = 2$  and for the limit of static disorder discussed in connection with Eq. (2.17). The constrained mean times are shown as differences from the unconstrained mean. The solid curves are calculated for a case in which the site state with the faster reaction rate has the slower product desorption rate:  $k_{D_1} = 0.1$ ,  $k_{D_2} = 0.01$ ,  $k_{L_1} = 1$ ,  $k_{L_2} = 10$ . The time unit is  $k_{L_1}^{-1}$ . All rate constants for interchange of site states are small enough not to contribute to the time dependences shown:  $l_{\alpha\gamma} = d_{\alpha\gamma} = 10^{-4}$ . The dashed curves are calculated with the values of  $k_{D_1}$  and  $k_{D_2}$  interchanged, and all other parameters with the same values, so that for this case, the site state with the faster reaction rate also has the faster product desorption rate. The algebraic signs of these quantities are shown to indicate correlations between rate constants for reaction and product desorption.

The plots in Fig. 2 were calculated for static disorder. The effects of increasing the rate constants for site state transitions to introduce dynamic disorder are shown in Fig. 3 which displays the four constrained mean dwell times for the same rate constants for reaction and desorption as used in the solid curves in Fig. 2. The solid curves in Fig. 3 repeat the solid curves from Fig. 2 with  $d_{\alpha\gamma} = l_{\alpha\gamma} = 10^{-4}$ . These rates are increased to  $d_{\alpha\gamma} = l_{\alpha\gamma} = 10^{-2}$  in the dashed curves and to  $d_{\alpha\gamma} = l_{\alpha\gamma} = 10^{-1}$  in the dotted curves. Increasing these rates decreases the time scales over which the constrained mean times are selective, resulting in more rapid decays. In addition, the initial amplitudes of  $\Delta\bar{t}_{D<}(\tau_L)$  and  $\Delta\bar{t}_{L<}(\tau_D)$  and the asymptotic large  $\tau_L$  or  $\tau_D$  limits of  $\Delta\bar{t}_{D>}(\tau_L)$  and  $\Delta\bar{t}_{L>}(\tau_D)$  decrease in absolute magnitude with increasing dynamic disorder. Figure 3 illustrates that even with dynamic disorder, the qualitative appearance of the static calculations in Fig. 2 can be preserved. However, if the rate constants  $d_{\alpha\gamma}$  and  $l_{\alpha\gamma}$  are much larger than the rate constants  $k_{D_\alpha}$  and  $k_{L_\alpha}$ , the constrained mean time differences need not decay monotonically, and can change algebraic sign, resulting in a qualitatively different appearance from Figs. 2 and 3. As shown below in Sec. IV, monotonic decays are indeed observed for the single-nanoparticle measurements of Refs. 23 and 28.

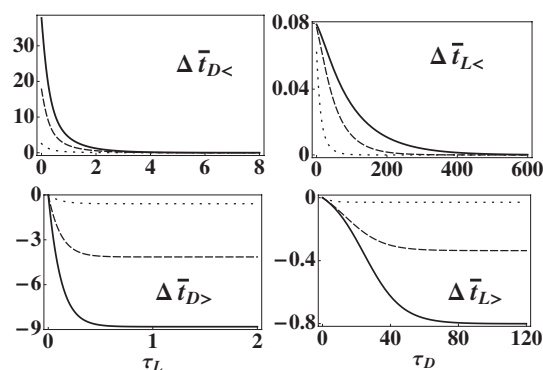


FIG. 3. Constrained mean dwell times are shown for a catalyst with one active site and two internal states. Differences between constrained and unconstrained mean times are plotted. Rate constants for reaction and desorption have the same values as the solid curves in Fig. 2,  $k_{D_1} = 0.1$ ,  $k_{D_2} = 0.01$ ,  $k_{L_1} = 1$ , and  $k_{L_2} = 10$ . Rate constants for changing site states  $d_{\alpha\gamma} = l_{\alpha\gamma}$  are increased from the value in Fig. 2 of  $10^{-4}$  (solid) to  $10^{-2}$  (dashes) to  $10^{-1}$  (dots). Time unit is  $k_{L_1}^{-1}$ .

### III. MULTIPLE ACTIVE SITES

We generalize the preceding model with a single active site to the case of  $N$  sites, and treat two limiting cases for the fluctuation dynamics. In the model of correlated fluctuations, all  $N$  sites occupy the same site state at any instant and change states together, while in the model of independent fluctuations, each of the  $N$  sites independently undergoes the single-site dynamics of Sec. II. In both models we restrict the state space to consider at most one site occupied by a product fluorescent molecule to conform to the experimental conditions of Chen and co-workers.<sup>23,28</sup> In the model of correlated fluctuations, the system has  $S$  nonfluorescent states  $\mathcal{D}_\alpha$ , in which each of the  $N$  sites has state  $D_\alpha$  for  $\alpha = 1, \dots, S$ . Each site has state  $\alpha$  and is occupied by an adsorbed reactant. There are  $NS$  fluorescent states  $\mathcal{L}_{\alpha j}$ , in which site  $j$  has state  $L_\alpha$  and all other sites have state  $D_\alpha$ . Each site has state  $\alpha$  and site  $j$  has a product molecule, with all other sites occupied by reactant. When only reactant molecules are adsorbed, all sites change state together from  $\gamma$  to  $\alpha$  with rate constant  $d_{\alpha\gamma}$  and when one product molecule is adsorbed, this rate constant is  $l_{\alpha\gamma}$ . The probabilities for nonfluorescent states are denoted  $P_{D_\alpha}(t)$  and for fluorescent states  $P_{L_{\alpha j}}(t)$ . The total probability that one product molecule is adsorbed to any site with the system in state  $\alpha$  is then given by  $P_{\mathcal{L}\alpha}(t) \equiv \sum_{j=1}^N P_{L_{\alpha j}}(t)$ . Dynamical equations for this model may be written in the same form as Eqs. (2.1) and (2.2) for  $N = 1$ , with renormalized rate constants:

$$|\dot{P}(t)\rangle = \tilde{\mathbf{w}}|P(t)\rangle, \quad (3.1)$$

$$\tilde{\mathbf{w}} = -\tilde{\mathbf{w}}_D - \mathbf{w}_L + \mathbf{w}_{DL} + \tilde{\mathbf{w}}_{LD}. \quad (3.2)$$

Here  $|P(t)\rangle$  is a  $2S$ -dimensional vector with elements  $P_{D_\alpha}(t)$  and  $P_{L_{\alpha j}}(t)$ ,  $\mathbf{w}_L$  and  $\mathbf{w}_{DL}$  are defined as for  $N = 1$  in Eq. (2.2), and  $\tilde{\mathbf{w}}_D$  and  $\tilde{\mathbf{w}}_{LD}$  differ only from  $\mathbf{w}_D$  and  $\mathbf{w}_{LD}$  for  $N = 1$  in that  $k_{D_\alpha}$  is replaced by  $Nk_{D_\alpha}$ . The model of  $N$  sites with correlated fluctuations is equivalent to that for a single site, with the reaction rate constant enhanced by a factor of  $N$ , since reaction may occur at any of the  $N$  sites. The definition and

analysis of the constrained mean dwell times  $\bar{t}_{L<}(\tau_D)$ ,  $\bar{t}_{L>}(\tau_D)$ ,  $\bar{t}_{D<}(\tau_L)$ , and  $\bar{t}_{D>}(\tau_L)$  follow as for  $N = 1$  in Sec. II with the only modification that  $k_{D\alpha} \rightarrow Nk_{D\alpha}$ .

For the model of  $N$  sites with independent fluctuations, the complete state space has dimension  $(2S)^N$  and is composed of  $S^N$  nonfluorescent states and  $(2S)^N - S^N$  fluorescent states. The fluorescent states that are accessed experimentally are the  $N S^N$  states in which a single product molecule is present. The full  $(2S)^N$ -dimensional vector of probabilities obeys the dynamical equation

$$|\dot{P}(t)\rangle = (-\mathbf{W}_D - \mathbf{W}_L + \mathbf{W}_{LD} + \mathbf{W}_{DL})|P(t)\rangle, \quad (3.3)$$

$$|P(t)\rangle \equiv \prod_{j=1}^N |p^{(j)}(t)\rangle, \quad (3.4)$$

$$\mathbf{W}_x = \sum_{j=1}^N \mathbf{w}_x^{(j)}. \quad (3.5)$$

In Eq. (3.4), the vector of multisite probabilities is written as a direct product of the probability vectors for each site  $j$ . Each  $|p^{(j)}(t)\rangle$  evolves according to the single-site dynamics in Eq. (2.1). In Eq. (3.5),  $\mathbf{W}_x$  represents  $\mathbf{W}_D$ ,  $\mathbf{W}_L$ ,  $\mathbf{W}_{LD}$ , or  $\mathbf{W}_{DL}$ , and is written as a sum over all sites of the corresponding single-site matrices in Eq. (2.2). Conditions of equilibrium and probability conservation, analogous to those for  $N = 1$  in Eqs. (2.3)–(2.7) with  $\mathbf{w}_x$  replaced by  $\mathbf{W}_x$  and  $|p\rangle$  replaced by  $|P\rangle$ , are valid here. We define idempotent projection matrices for the  $N$  site system as direct products of the single-site projectors  $\mathbf{s}_D$  and  $\mathbf{s}_L$ , defined preceding Eq. (2.3),

$$\mathbf{S}_D \equiv \prod_{j=1}^N \mathbf{s}_D^{(j)}, \quad (3.6)$$

$$\mathbf{S}_{IL} \equiv \sum_{i=1}^N \prod_{j \neq i} \mathbf{s}_L^{(i)} \mathbf{s}_D^{(j)}, \quad (3.7)$$

where, for example,  $\mathbf{s}_D^{(j)}$  acts on states of site  $j$ . The matrix  $\mathbf{S}_D$  projects into the subspace of states in which all sites are D, and  $\mathbf{S}_{IL}$  projects into the experimentally accessed subspace of states in one site is L and the rest are D.

The distribution of dwell times in a fluorescent state in which one site is occupied by a product molecule and the rest are occupied by reactants is given, by analogy to the  $N = 1$  case in Eq. (2.8), by

$$F_L(t_L) \equiv \frac{\langle I | \mathbf{W}_{DL} e^{-\mathbf{W}_L t_L} \mathbf{W}_{LD} | P \rangle}{\langle I | \mathbf{W}_{DL} | P \rangle}, \quad (3.8)$$

with  $\langle I |$  the direct product of site vectors  $\langle 1 |$  is defined following Eq. (2.6). This result may be simplified by defining a dynamical matrix  $\mathbf{\Omega}_L = \mathbf{S}_{IL} \mathbf{W}_L \mathbf{S}_{IL}$  that acts only in the subspace of fluorescent states in which a single site is occupied by a fluorescent product molecule. The matrix  $\mathbf{\Omega}_L$  describes dynamics at the single site with adsorbed product, either desorption or changes in site state, and no dynamics at the other sites occupied by reactants. Its action can be related to that of the full dynamical matrix in the space of all fluorescent states  $\mathbf{W}_L$ . In particular,  $\mathbf{W}_L | P \rangle = \mathbf{\Omega}_L | P \rangle$ , which can be verified as follows. Because of the equilibrium condition,  $\mathbf{W}_L | P \rangle$

$= \mathbf{W}_{LD} | P \rangle$ , which is

$$\begin{aligned} \sum_{i=1}^N \mathbf{w}_{LD}^{(i)} | p^{(i)} \rangle \prod_{j \neq i} \mathbf{s}_D^{(j)} | p^{(j)} \rangle &= \sum_{i=1}^N \mathbf{w}_L^{(i)} | p^{(i)} \rangle \prod_{j \neq i} \mathbf{s}_D^{(j)} | p^{(j)} \rangle \\ &= \sum_{i=1}^N \mathbf{w}_L^{(i)} \mathbf{S}_{IL} | P \rangle \equiv \mathbf{\Omega}_L | P \rangle. \end{aligned} \quad (3.9)$$

The first equality in Eq. (3.9) follows from the equilibrium condition for a single site in Eq. (2.4), and the second equality from the definition of the projector  $\mathbf{S}_{IL}$  in Eq. (3.7). It is also the case that  $\langle I | \mathbf{W}_L = \langle I | \mathbf{\Omega}_L$ ,

$$\begin{aligned} \langle I | \mathbf{W}_L &= \langle I | \mathbf{W}_{DL} = \sum_{i=1}^N \prod_{j \neq i} \langle 1^{(j)} | \mathbf{s}_D^{(j)} \langle 1^{(i)} | \mathbf{w}_{DL}^{(i)} \\ &= \sum_{i=1}^N \prod_{j \neq i} \langle I | \mathbf{S}_{IL} \mathbf{w}_L^{(i)} = \langle I | \mathbf{\Omega}_L. \end{aligned} \quad (3.10)$$

These equalities permit the distribution of dwell times in the fluorescent state for  $N$  sites in Eq. (3.8) to be readily expressed in terms of properties of a single site,

$$F_L(t_L) = \frac{d^2 G_L(t_L)}{dt_L^2}, \quad (3.11)$$

$$G_L(t_L) \equiv \frac{\langle I | \mathbf{S}_{IL} e^{-\mathbf{\Omega}_L t_L} \mathbf{S}_{IL} | P \rangle}{\langle I | \mathbf{\Omega}_L | P \rangle} = g_L(t_L). \quad (3.12)$$

The second equality in Eq. (3.12) follows from the definition of  $\mathbf{\Omega}_L$  and shows that  $G_L(t_L)$  is independent of  $N$  for this model. Therefore, under the condition that at most one site holds a fluorescent product molecule, the distribution of dwell times in the fluorescent state for  $N$  sites is the same as the result for one site, given in Eq. (2.9) with L replacing D.

In contrast to the distribution of  $t_L$ , the distribution of  $t_D$  for  $N$  independently fluctuating sites does depend on  $N$ ,

$$F_D(t_D) = \frac{\langle I | \mathbf{W}_{LD} e^{-\mathbf{W}_D t_D} \mathbf{W}_{DL} | P \rangle}{\langle I | \mathbf{W}_{DL} | P \rangle} = \frac{\partial^2}{\partial t_D^2} G_D(t_D), \quad (3.13)$$

$$\begin{aligned} G_D(t_D) &\equiv \frac{\langle I | \mathbf{S}_D e^{-\mathbf{W}_D t_D} \mathbf{S}_D | P \rangle}{\langle I | \mathbf{W}_D | P \rangle} \\ &= g_D(t_D) \frac{(E_D(t_D))^{N-1}}{N}, \end{aligned} \quad (3.14)$$

$$E_D(t_D) \equiv \frac{\langle 1 | \mathbf{s}_D e^{-\mathbf{w}_D t_D} \mathbf{s}_D | p \rangle}{\langle 1 | \mathbf{s}_D | p \rangle}. \quad (3.15)$$

In Eq. (3.14), the generating function for  $N$  sites  $G_D(t_D)$  is written in terms of that for one site  $g_D(t_D)$ , defined as in Eq. (2.10). The  $N$ -dependence of this generating function originates in the dynamics of each of the  $N$  adsorbed reactants having the possibility of undergoing chemical reaction.  $E_D$  defined in Eq. (3.15) is a normalized decay reflecting the averaged reaction dynamics at a single site. In the large  $N$  limit,

$(E_D(t_D))^N$  can be evaluated through a first-order cumulant approximation to  $E_D$  with a quadratic correction,

$$(E_D(t_D))^N \approx \exp(-N t_D / \bar{t}_D) \left(1 + N \sigma_{w_D}^2 t_D^2 / 2 + \dots\right), \quad (3.16)$$

$$\sigma_{w_D}^2 \equiv \frac{\langle 1 | \mathbf{w}_D^2 | p \rangle}{\langle 1 | \mathbf{s}_D | p \rangle} - (\bar{t}_D)^{-2}, \quad (3.17)$$

with  $\bar{t}_D$  referring to a single site. For large  $N$ ,  $(E_D(t_D))^{N-1} \approx \exp(-N t_D / \bar{t}_D)$ , since in this limit the quadratic correction for  $t_D \approx \bar{t}_D / N$  is of order  $N^{-1}$ , and therefore negligible.

The joint distributions of successive dwell times are defined by analogy with the single-site case in Eq. (2.12), and are related to single-site quantities by

$$F_{DL}(t_D, t_L) = \frac{\partial^2}{\partial t_L \partial t_D} G_{DL}(t_D, t_L), \quad (3.18)$$

$$G_{DL}(t_D, t_L) \equiv \frac{\langle I | \mathbf{S}_D e^{-\mathbf{W}_D t_D} \mathbf{W}_{DL} e^{-\Omega_L t_L} \mathbf{S}_{IL} | P \rangle}{\langle I | \mathbf{W}_{LD} | P \rangle} = g_{DL}(t_D, t_L) (E_D(t_D))^{N-1}, \quad (3.19)$$

$$F_{LD}(t_L, t_D) = \frac{\partial^2}{\partial t_L \partial t_D} G_{LD}(t_L, t_D), \quad (3.20)$$

$$G_{LD}(t_L, t_D) \equiv \frac{\langle I | \mathbf{S}_{IL} e^{-\Omega_L t_L} \mathbf{W}_{LD} e^{-\mathbf{W}_D t_D} \mathbf{S}_D | P \rangle}{\langle I | \mathbf{W}_{LD} | P \rangle} = g_{LD}(t_L, t_D) (E_D(t_D))^{N-1}. \quad (3.21)$$

The generating functions for  $N$  independent sites  $G_{DL}$  and  $G_{LD}$  are modified from their  $N = 1$  forms by the normalized decay factor  $(E_D(t_D))^{N-1}$ . The constrained mean times are defined similarly to the  $N = 1$  case in, e.g., Eq. (2.15). The mean time in the fluorescent state given that the previous time in the nonfluorescent state is less than a specified value is related to single-site dynamical quantities by

$$\bar{t}_{L<}(\tau_D) \equiv \frac{\int_0^\infty dt_L t_L \int_0^{\tau_D} dt_D F_{LD}(t_L, t_D)}{\int_0^{\tau_D} dt_D F_D(t_D)}, \quad (3.22)$$

$$\Delta \bar{t}_{L<}(\tau_D) = (E_D(\tau_D))^{N-1} \times \left( \frac{-\bar{t}_L \dot{g}_D(\tau_D) - \int_0^\infty dt_L g_{LD}(t_L, \tau_D)}{1 + (E_D(\tau_D))^{N-1} \dot{g}_D(\tau_D)} \right). \quad (3.23)$$

At  $N = 1$  this reduces to the single-site expression in Eq. (2.16). For  $S = 2$  and static disorder, as in Eq. (2.17), Eq. (3.23) becomes

$$\Delta \bar{t}_{L<}(\tau_D) = \left( \frac{e^{-N \tau_D / \bar{t}_D} p_{L_1} p_{L_2}}{\langle 1 | \mathbf{w}_L | p \rangle} \right) \left( \frac{(k_{L_1} - k_{L_2}) (e^{-k_{D_1} \tau_D} - e^{-k_{D_2} \tau_D})}{(1 - e^{-k_{D_1} \tau_D} e^{-N \tau_D / \bar{t}_D}) k_{D_1} p_{D_1} + (1 - e^{-k_{D_2} \tau_D} e^{-N \tau_D / \bar{t}_D}) k_{D_2} p_{D_2}} \right). \quad (3.24)$$

This expression includes the first-order cumulant approximation in Eq. (3.16).  $\Delta \bar{t}_{L<}(\tau_D)$  decays to zero from either a positive or a negative initial value. The sign of  $\Delta \bar{t}_{L<}(\tau_D)$  is determined by the identical criteria discussed for the  $N = 1$  case in Eq. (2.17). For a separation of time scales in reaction rates,  $k_D^{\text{big}} \gg k_D^{\text{small}}$ , for  $N = 1$ , the asymptotic decay rate is  $k_D^{\text{big}}$ . For  $N$  sites in Eq. (3.24), the asymptotic decay rate is approximately larger by a factor of  $N$ ,  $N / \bar{t}_D \approx N k_D^{\text{big}}$ . The conjugate constrained mean time in the fluorescent state given that the preceding time in the nonfluorescent state exceeds  $\tau_D$  is defined for  $N$  independent sites as

$$\bar{t}_{L>}(\tau_D) \equiv \frac{\int_0^\infty dt_L t_L \int_{\tau_D}^\infty dt_D F_{LD}(t_L, t_D)}{\int_{\tau_D}^\infty dt_D F_D(t_D)}. \quad (3.25)$$

The decay factor  $(E_D(\tau_D))^{N-1}$  in Eq. (3.23) enters multiplicatively in both numerator and denominator of this expression, and cancels leaving a result independent of  $N$  and therefore equals to the  $N = 1$  result in Eq. (2.19).

The mean time in the nonfluorescent state given that the preceding time in the fluorescent state does not exceed a value

$\tau_L$  is written in terms of single-site dynamics as

$$\Delta \bar{t}_{D<}(\tau_L) = \frac{-\bar{t}_D \dot{g}_L(\tau_L) / N - \int_0^\infty dt_D g_{DL}(t_D, \tau_L) (E_D(t_D))^{N-1}}{1 + \dot{g}_L(\tau_L)}. \quad (3.26)$$

In the  $N \rightarrow \infty$  limit, this quantity must vanish at all times, because in this model there is no correlation between a product desorption event at one site, which terminates a fluorescent period, and a chemical reaction at a different site that terminates the following nonfluorescent period. Demonstrating this  $N$  dependence requires including the quadratic correction in Eq. (3.16). For two states and in the limit of static disorder,  $\Delta \bar{t}_{D<}(\tau_L)$  for  $N$  sites is related to that for one site by

$$\Delta \bar{t}_{D<}(\tau_L) \approx k_{D_1} k_{D_2} \left( \frac{\bar{t}_D}{N} \right)^2 (\Delta \bar{t}_{D<}(\tau_L))_{N=1}. \quad (3.27)$$

This result does not reduce to the single-site result for  $N = 1$  as it only holds for large  $N$ .  $\Delta \bar{t}_{D<}(\tau_L)$  has the same algebraic sign and decay rates as for  $N = 1$  but with reduced amplitude reflecting the contributions from uncorrelated events at different sites. The conjugate constrained mean time in the nonfluorescent state given that the preceding time in the fluorescent

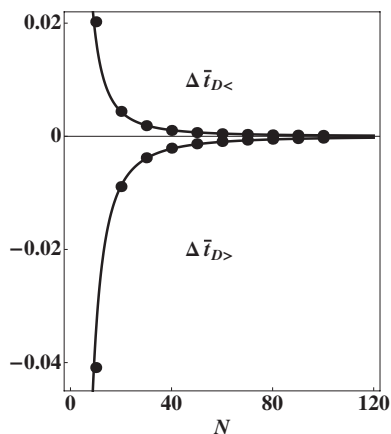


FIG. 4. Discrete points show constrained mean dwell time differences in the nonfluorescent state at  $\tau_L = 1$  for catalysts with  $N$  active sites, each with two internal states. Rate constants for reaction and desorption have the same values as the solid curves in Fig. 2,  $k_{D_1} = 0.1$ ,  $k_{D_2} = 0.01$ ,  $k_{L_1} = 1$ , and  $k_{L_2} = 10$ , as do rate constants for changing site states,  $d_{\alpha\gamma} = l_{\alpha\gamma} = 10^{-4}$ . Solid curves are fits to the form  $\propto N^{-2}$ . Time unit is  $k_{L_1}^{-1}$ .

state exceeds  $\tau_L$  is

$$\Delta\bar{\tau}_{D>}(\tau_L) = \frac{-\bar{\tau}_D \dot{g}_L(\tau_L)/N - \int_0^\infty dt_D g_{DL}(t_D, \tau_L)(E_D(t_D))^{N-1}}{\dot{g}_L(\tau_L)}. \quad (3.28)$$

In the static limit for two states and for  $N \gg 1$ ,  $\Delta\bar{\tau}_{D>}(\tau_L)$  is related to the mean time for a single site by the same factor as in Eq. (3.27),

$$\Delta\bar{\tau}_{D>}(\tau_L) \approx k_{D_1} k_{D_2} \left(\frac{\bar{\tau}_D}{N}\right)^2 (\Delta\bar{\tau}_{D>}(\tau_L))_{N=1}. \quad (3.29)$$

The algebraic sign and decay times are the same as for  $N = 1$ , but the amplitude is reduced by the same factor of  $N^2$  as in Eq. (3.27). The validity of Eqs. (3.27) and (3.29) is assessed in Fig. 4, which shows the  $N$ -dependence of  $\Delta\bar{\tau}_{D<}(\tau_L)$  and  $\Delta\bar{\tau}_{D>}(\tau_L)$  at  $\tau_L = 1$  for the model of independent fluctuations with the same parameters used in the solid curves of Fig. 2. Discrete points show exact results, and the solid curves show numerical fits to  $\propto N^{-2}$ . Large  $N$  behavior is shown to be valid for  $N$  as small as 10.

We can now compare qualitatively the four constrained mean times for  $N$  active sites with either correlated or independent site state fluctuations. For simplicity, we consider the limit treated in Fig. 4 with  $S = 2$  and static disorder. We consider two attributes: the algebraic signs of the constrained mean time differences and the asymptotic decay rates, assuming a separation of time scales in both reaction and desorption dynamics,  $k_D^{\text{big}} \gg k_D^{\text{small}}$  and  $k_L^{\text{big}} \gg k_L^{\text{small}}$ . Both models predict the same algebraic signs of the four constrained mean time differences, which are as shown for  $N = 1$  in Fig. 2. Thus these algebraic signs are insensitive to correlations among dynamic fluctuations. The asymptotic decay rate for  $\Delta\bar{\tau}_{D<}(\tau_L)$  is  $k_L^{\text{small}}$  for both models, and that for  $\Delta\bar{\tau}_{D>}(\tau_L)$  is  $k_L^{\text{big}}$  for both models. Qualitative analysis of the constrained mean times in the dark state does not allow a simple distinction between the two models. However, the two models differ in the decay rates for constrained mean times in the light state. In

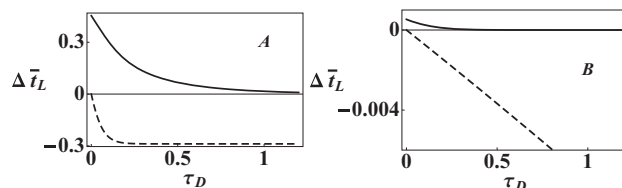


FIG. 5. Constrained mean dwell times in the fluorescent state are shown for a catalyst with  $N = 256$  active sites, each with two internal states. Differences between constrained and unconstrained mean times are plotted. Rate constants for reaction and desorption have the same values as the solid curves in Fig. 2,  $k_{D_1} = 0.1$ ,  $k_{D_2} = 0.01$ ,  $k_{L_1} = 1$ , and  $k_{L_2} = 10$ , as do rate constants for changing site states,  $d_{\alpha\gamma} = l_{\alpha\gamma} = 10^{-4}$ . In panel A, all sites change states simultaneously, while in panel B, sites change states independently. Solid lines show  $\Delta\bar{\tau}_{L<}(\tau_D)$  and dashes show  $\Delta\bar{\tau}_{L>}(\tau_D)$ . Time unit is  $k_{L_1}^{-1}$ .

the model of correlated fluctuations,  $\Delta\bar{\tau}_{L<}(\tau_D)$  has asymptotic decay rate  $Nk_D^{\text{small}}$  and  $\Delta\bar{\tau}_{L>}(\tau_D)$  has asymptotic decay rate  $Nk_D^{\text{big}}$ . In the model of independent fluctuations,  $\Delta\bar{\tau}_{L<}(\tau_D)$  has asymptotic decay rate  $Nk_D^{\text{big}}$  and  $\Delta\bar{\tau}_{L>}(\tau_D)$  has asymptotic decay rate  $k_D^{\text{big}}$ . Thus, for large  $N$  and in the static limit  $\Delta\bar{\tau}_{L<}(\tau_D)$  decays more slowly than  $\Delta\bar{\tau}_{L>}(\tau_D)$  for correlated fluctuations, but  $\Delta\bar{\tau}_{L<}(\tau_D)$  decays more rapidly than  $\Delta\bar{\tau}_{L>}(\tau_D)$  for independent fluctuations. These differing predictions are illustrated in Fig. 5, which shows  $\Delta\bar{\tau}_{L<}(\tau_D)$  (solid lines) and  $\Delta\bar{\tau}_{L>}(\tau_D)$  (dashed lines) for  $k_{D_1} = 0.1$ ,  $k_{D_2} = 0.01$ ,  $k_{L_1} = 1$ , and  $k_{L_2} = 10$  with  $l_{\alpha\gamma} = d_{\alpha\gamma} = 10^{-4}$  for  $N = 256$  active sites. Panel A was calculated for correlated fluctuations, and panel B shows results for independent fluctuations. In panel A,  $\Delta\bar{\tau}_{L>}(\tau_D)$  has the faster decay, while in panel B,  $\Delta\bar{\tau}_{L<}(\tau_D)$  decays more quickly. If experimental data show that one of  $\Delta\bar{\tau}_{L<}(\tau_D)$  or  $\Delta\bar{\tau}_{L>}(\tau_D)$  decays significantly more rapidly than the other, it will be possible to determine which of these models is the more appropriate description.

The two models of correlated and independent fluctuations are limiting cases of a more general model that interpolates between these limits. Here the  $N$  sites are composed of  $J$  domains each of identical size  $M$ , so that  $N = JM$ . Site states fluctuate in a correlated fashion within a domain, but no correlation exists between domains. Constrained mean dwell times for this model may be obtained from results already presented as follows. A result for the domain model is obtained from the corresponding quantity for the model of independent fluctuations by replacing the number of sites  $N$  with the number of domains  $J$  and replacing all single-site quantities with the corresponding result for the correlated fluctuation model with  $N$  replaced by  $M$ . With this procedure, the asymptotic decay rate for  $\Delta\bar{\tau}_{L<}(\tau_D)$  becomes approximately  $(J-1)Mk_D^{\text{big}} + Mk_D^{\text{small}}$ . This result is correct at  $J = 1$  and for  $J \gg 1$ , but not necessarily for intermediate values. For  $J = 1$  and  $M = N$ , the result for the correlated model  $Nk_D^{\text{small}}$  is recovered, while for  $J = N$  and  $M = 1$  the result for the model of independent fluctuations  $(N-1)k_D^{\text{big}} \rightarrow Nk_D^{\text{big}}$  is obtained. The asymptotic decay rate for the conjugate time  $\Delta\bar{\tau}_{L>}(\tau_D)$  is  $Mk_D^{\text{big}}$ , which likewise interpolates between the correlated fluctuation result of  $Nk_D^{\text{big}}$  and the independent fluctuation result of  $k_D^{\text{big}}$ . Since the two limiting models make opposite predictions for which of  $\Delta\bar{\tau}_{L<}(\tau_D)$  and  $\Delta\bar{\tau}_{L>}(\tau_D)$  decays most rapidly, the domain model must display a crossover such that

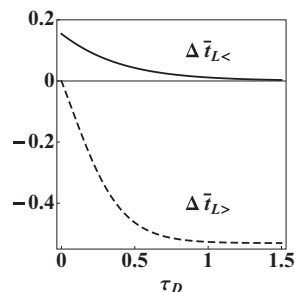


FIG. 6. Constrained mean dwell times in the fluorescent state are shown for a catalyst with  $N = 256$  active sites, each with two internal states. Differences between constrained and unconstrained mean times are plotted. All rate constants are identical to those in Fig. 5. The system is composed of 4 domains of 64 sites each, with site fluctuations correlated within a domain and uncorrelated between domains. Time unit is  $k_{L1}^{-1}$ .

for certain values of  $J$  and  $M$ , the two times have similar decay rates. Such dynamics are shown in Fig. 6 in which the number of sites and rate constant values are identical to those in Fig. 5, but with  $J = 4$  equivalent domains of size  $M = 64$ . For this case,  $\Delta\bar{\tau}_{L<}(\tau_D)$  and  $\Delta\bar{\tau}_{L>}(\tau_D)$  have comparable decay times.

#### IV. SINGLE TURNOVER NANOPARTICLE MEASUREMENTS

We have calculated constrained mean dwell times from single-turnover fluorescence trajectories measured by Chen and co-workers<sup>23,28</sup> for the reductive  $N$ -deoxygenation of the nonfluorescent reactant resazurin to the fluorescent product resorufin, catalyzed by a spherical gold nanoparticle. Constrained mean dwell times were computed from trajectories for individual nanoparticles, and then averaged over the ensemble of trajectories for nanoparticles of the same diameter and with the same reactant concentrations. At least 50 trajectories were averaged for each diameter. The mean dwell times  $\bar{\tau}_L$  and  $\bar{\tau}_D$  show saturation behavior as a function of reactant concentration,<sup>23,28</sup> and only data in the saturation regime are analyzed here. Results are presented in Figure 7 for diameters and resazurin concentrations  $6.0 \pm 1.7$  nm and  $1.2 \mu\text{M}$  (solid lines),  $9.1 \pm 1.5$  nm and  $0.4 \mu\text{M}$  (dotted lines), and  $13.7 \pm 2.4$  nm and  $0.4 \mu\text{M}$  (dashed lines). All times are given in seconds. Zhou *et al.*<sup>28</sup> observed a significant difference between the catalytic deactivation of particles with the smallest diameter and with the two larger diameters. For particles of the two larger diameters,  $\bar{\tau}_D$  is found to increase during the course of the measurement on the time scale of tens of minutes, indicating that the catalyst becomes deactivated in time. Since  $\bar{\tau}_L$  does not show this time dependence, poisoning of the catalyst by reaction products other than resorufin has been proposed as a cause.<sup>28</sup> For the 6 nm diameter particles, such deactivation occurs detectably only on times longer than three hours, providing a sufficient time window to collect data without significant deactivation. The curves in Fig. 7 for the three particle diameters have the same algebraic sign and qualitative appearance. The models of Secs. II and III could be modified to include an irreversible deactivation process when a site is in the dark state. However, to simplify the interpretation, we

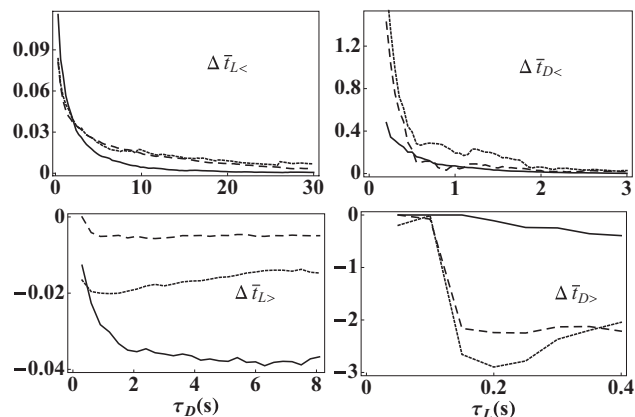


FIG. 7. Constrained mean dwell times are calculated from single-turnover measurements of the catalysis by spherical gold nanoparticles of the conversion of resazurin to resorufin. The nanoparticle diameter is varied from 6.0 nm (solid lines) to 9.1 nm (dotted lines) to 13.7 nm (dashed lines).

will focus attention on the data for the particles with 6 nm diameter for which deactivation is negligible.

The data in Fig. 7 for particles of diameter 6 nm are re-plotted as the open squares in Fig. 8. As in Fig. 7, all times are given in seconds. Dashed curves show fits to empirical functional forms,  $\Delta\bar{\tau}_{j<}(\tau) = C_1 e^{-k_1 \tau} + C_2 e^{-k_2 \tau}$  and  $\Delta\bar{\tau}_{j>}(\tau) = C_3 (1 - e^{-k_3 \tau}) / (C_4 + e^{-k_3 \tau})$ . For  $j = L$ ,  $C_1 = 0.0426$  s,  $C_2 = 0.104$  s,  $C_3 = -0.0744$  s,  $C_4 = 2.00$ ,  $k_1 = 0.217$  s<sup>-1</sup>,  $k_2 = 1.18$  s<sup>-1</sup>,  $k_3 = 1.835$  s<sup>-1</sup>. For  $j = D$ ,  $C_1 = 0.373$  s,  $C_2 = 0.926$  s,  $C_3 = -0.0287$  s,  $C_4 = 0.0477$ ,  $k_1 = 1.66$  s<sup>-1</sup>,  $k_2 = 7.83$  s<sup>-1</sup>,  $k_3 = 9.37$  s<sup>-1</sup>. In Sec. III, we demonstrated that constrained mean dwell times are sensitive to correlations among dynamic fluctuations at different active sites in a catalyst with multiple active sites. In particular, we showed that for  $N$  sites with completely correlated fluctuations,  $\Delta\bar{\tau}_{L>}(\tau_D)$  decays more rapidly than  $\Delta\bar{\tau}_{L<}(\tau_D)$ , while for completely independent fluctuations,  $\Delta\bar{\tau}_{L>}(\tau_D)$  decays more slowly than  $\Delta\bar{\tau}_{L<}(\tau_D)$ . A qualitative comparison of these two quantities indicates the importance of dynamic correlations among events at different active sites. These two quantities for 6 nm particles are shown in the two left-hand panels of Fig. 8, which demonstrate that  $\Delta\bar{\tau}_{L>}(\tau_D)$  decays more rapidly than  $\Delta\bar{\tau}_{L<}(\tau_D)$ . Similar trends are also clear for gold nanoparti-

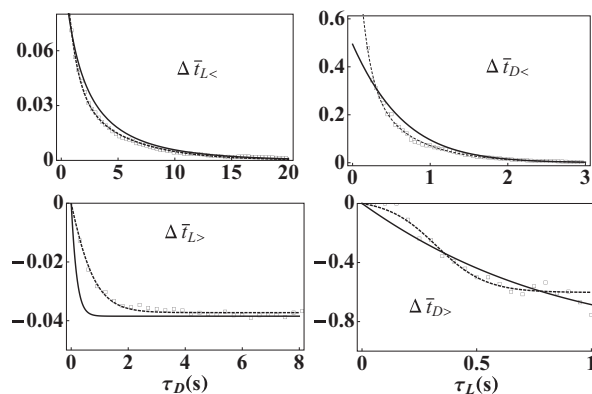


FIG. 8. Constrained mean dwell times are shown as open squares for gold nanoparticles of diameter 6 nm. Dashed lines show empirical fits and solid lines show fits to a two-state kinetic model with dynamic disorder.

cles of diameter 9 and 14 nm, as shown in Fig. 7. These data are thus more consistent with a scenario in which state fluctuations among active sites are correlated, than with a picture in which the fluctuations occur entirely independently. In Sec. III, we showed that in the model of completely correlated fluctuations, the number of active sites  $N$  enters only as a scaling factor multiplying rate constants, so that in principle the data in Fig. 8 are also consistent with the case of  $N = 1$ , with each nanoparticle having a single active site. However, this is not the case, since several product molecules are occasionally observed<sup>23</sup> simultaneously on single 6 nm nanoparticles, indicating the presence of a multiplicity of sites. The present analysis therefore indicates correlated dynamics at active sites on gold nanoparticles.

The solid curves in Fig. 8 show least-squares fits to the predictions of the kinetic model of Sec. III with  $S = 2$ ,  $N$  sites, and completely correlated fluctuations. The limit of static disorder is not assumed to hold, so that, for example,  $\Delta\bar{t}_{L <}(\tau_D)$  is calculated from the general form in Eq. (2.16) rather than from the simplified static limit in Eq. (2.17). The resulting parameter values are  $Nk_{D_1} = 6.30 \text{ s}^{-1}$ ,  $Nk_{D_2} = 0.176 \text{ s}^{-1}$ ,  $k_{L_1} = 1.45 \text{ s}^{-1}$ ,  $k_{L_2} = 2.48 \text{ s}^{-1}$ ,  $d_{12} = 0$ ,  $d_{21} = 0.147 \text{ s}^{-1}$ ,  $l_{12} = 0.516 \text{ s}^{-1}$ ,  $l_{21} = 0.861 \text{ s}^{-1}$ . The fit was carried out subject to the conditions that the unconstrained mean dwell times be near to the experimental values  $\bar{t}_L = 0.48 \text{ s}$  and  $\bar{t}_D = 4.28 \text{ s}$ . The solid curves in Fig. 8 yield unconstrained mean times  $\bar{t}_L = 0.47 \text{ s}$  and  $\bar{t}_D = 4.31 \text{ s}$ , close to the correct values. The fitted rate constant values describe a system near to the limit of static disorder, in which rate constants for site state changes,  $l_{\alpha\gamma}$  and  $d_{\alpha\gamma}$  are small compared to rate constants for reaction  $k_{D_\alpha}$  and product desorption  $k_{L_\gamma}$ . In particular, the rate constant for leaving a particular state because of changes in site state is smaller than the rate constant for leaving that state because of reaction or desorption, for example,  $l_{12} < k_{L_2}$ . Figure 8 demonstrates that a two-state model provides a qualitatively reasonable but not a quantitative fit to constrained mean dwell times for single nanoparticles.

The applicability of the  $S = 2$  model to nanoparticle catalysis and the significance of the values of the fitted rate constants in Fig. 8 may be further assessed by considering another quantity that is extracted from binary fluorescence trajectories, the dwell time autocorrelation function<sup>1,5,15,23,36,37,62</sup>  $C_j(n)$  with  $j$  indicating D or L,

$$C_j(n) \equiv \overline{t_j(1)t_j(n+1)} - \bar{t}_j^2. \quad (4.1)$$

Here  $t_j(1)$  is a particular dwell time in state  $j$  in a fluorescence trajectory and  $t_j(n+1)$  is the dwell time in the same state that occurs immediately after the next  $n$  dwell times in the other state. In the absence of any disorder, this quantity vanishes, and in the presence of static disorder, it is independent of  $n$ . The decay of  $C_j(n)$  to zero with increasing  $n$  indicates the presence of dynamic disorder. For the  $S = 2$  model, these two normalized autocorrelation functions are identical.<sup>5,15</sup> As the static limit is approached and for  $n \gg 1$ , the two autocorrelation functions take the form<sup>5,15</sup>

$$\frac{C_L(n)}{C_L(1)} = \frac{C_D(n)}{C_D(1)} \approx e^{-n/n_0}, \quad (4.2)$$

$$\frac{1}{n_0} = \frac{d_{12}}{k_{D_2}} + \frac{d_{21}}{k_{D_1}} + \frac{l_{12}}{k_{L_2}} + \frac{l_{21}}{k_{L_1}}. \quad (4.3)$$

The reciprocal of the characteristic number of turnovers  $n_0$  that quantifies the decay of the autocorrelation functions is written in Eq. (4.3) as the sum of ratios of a rate constant representing probability loss out of a particular state from changes in site state ( $d_{\alpha\gamma}$  or  $l_{\alpha\gamma}$ ) to a rate constant representing probability loss from that same state because of either reaction or desorption ( $k_{D_\gamma}$  or  $k_{L_\gamma}$ ).

Xu *et al.*<sup>23</sup> determined that for a nanoparticle with diameter 6 nm,  $C_D(n)$  and  $C_L(n)$  decay exponentially with  $n_0$  taking on the values 12.5 and 2.6 for D and L, respectively. Three conclusions may be drawn from this experimental finding. First, because these autocorrelation functions decay with increasing  $n$ , the nanoparticle catalytic dynamics are characterized by dynamic disorder. Second, because  $n_0 > 1$  in each case, the processes that lead to dynamic disorder are slow relative to reaction and desorption of product. Third, since  $C_D(n)$  and  $C_L(n)$  decay differently, these kinetics cannot be fully modeled with a model of discrete dynamic disorder with only two states. As shown in Eqs. (4.2) and (4.3), for this case these two autocorrelation functions would decay identically with  $n$ . For  $S > 2$ , this model can yield dwell time autocorrelation functions with differing decay rates. The  $S = 2$  model provides a reasonable qualitative interpretation for the constrained dwell times, but a simultaneous description of the dwell time autocorrelation functions would require expanding the model to include additional site states. A complete analysis of the measured dwell time correlation functions is deferred to future work. However, the values of the rate constants used in the solid curves in Fig. 8 are in qualitative agreement with the correlation function data in the sense that rate constants for site state changes are smaller than those for reaction and product desorption, confirming that the kinetics are near the limit of static disorder.

Constrained mean dwell times calculated from the nanoparticle data support the interpretation of the autocorrelation function results in Ref. 23 that adsorption sites exist in several functionally different types. Figures 7 and 8 show that  $\Delta\bar{t}_{L <}(\tau_D)$  and  $\Delta\bar{t}_{D <}(\tau_L)$  decay to zero from positive values and that  $\Delta\bar{t}_{L >}(\tau_D)$  and  $\Delta\bar{t}_{D >}(\tau_L)$  decay from zero to negative asymptotes. As shown by the calculations in Fig. 2, these signs indicate that the rate at which a reactant molecule undergoes the catalytic reaction is inversely correlated with the rate of desorption of the resulting product molecule; a relatively rapid reaction event produces a relatively slowly desorbing product molecule. This qualitative conclusion is supported by the values of the rate constants used to generate the solid curves in Fig. 8. In these fits to the  $S = 2$  model,  $k_{D_1} > k_{D_2}$ , so site state 1 has the more rapid reaction, but  $k_{L_1} < k_{L_2}$  so site state 1 has slower desorption. This finding is consistent with a scenario in which reactions with lower activation barriers produce more stable surface-bound species.

The constrained mean dwell times also confirm the interpretation of the autocorrelation functions<sup>23,28</sup> in indicating the presence of dynamical processes that alter the condition of adsorbed reactants and products. These dynamics may arise in principle either from a mechanism in which the adsorption

sites change identity through surface reconstruction of the nanoparticle<sup>32–35</sup> or from a mechanism in which the sites are static, but mobile adsorbates can sample sites of different types,<sup>63</sup> or from some combination of these two limiting cases. The present analysis does not distinguish between dynamics of the nanoparticle and dynamics of adsorbates. Xu *et al.*<sup>23</sup> have measured the dependence of decay times of  $C_L(n)$  and  $C_D(n)$  on turnover rate. These autocorrelation functions decay increasingly rapidly as the reactant concentration is increased, consistent with a scenario of adsorbate-induced surface restructuring and not with dynamics arising from motion of reactant molecules. Raising reactant concentration increases the fraction of filled sites, hindering possible relaxation through translational motion. This interpretation of dynamic disorder arising from surface reconstruction is further supported by the observation that autocorrelation function decay rates decrease with increasing particle diameter.<sup>28</sup> Our finding that dynamical fluctuations at different active sites are correlated is also consistent with the surface reconstruction mechanism, as surface dynamics in metal nanoparticles can involve the entire particle, and are thus nonlocal.<sup>35</sup> The constrained mean dwell time analysis of single nanoparticle fluorescence turnover trajectories quantifies the role of disorder and of dynamical fluctuations in these kinetics.

## V. CONCLUSIONS

The analysis of binary fluorescence trajectories requires the identification of quantities that emphasize different aspects of the underlying kinetics.<sup>4,5,8,11–15,18,19,36–58</sup> Correlation functions of dwell times have been demonstrated previously to provide a direct probe of the dynamical processes that alter reactivity.<sup>6,23</sup> The constrained mean dwell times discussed here provide complementary information in emphasizing correlations between rates of reaction and rates of desorption and additionally identifying the presence of correlated fluctuations among distinct active sites. Consistency between binary fluorescence trajectories and a proposed kinetic scheme can be rigorously tested by requiring the model to predict correctly both dwell-time correlation functions and constrained mean dwell times.

Our constrained mean dwell time analysis of single nanoparticle kinetic data with a model of discrete states and dynamic disorder confirms that active sites exist in several states. States associated with rapid reaction are associated with slow desorption of the resulting product. These states interconvert through a dynamical process producing fluctuations that are correlated among several active sites. Laboratory observations<sup>23,28</sup> are consistent with the interpretation that these dynamics result from surface reconstruction of the nanoparticle.<sup>32–35</sup> Our results are based on a phenomenological kinetic model that does not address the microscopic nature of the disorder in active sites nor of the dynamical processes that affect them. Our findings, such as the inverse correlation of reaction rate constant with product desorption rate constant, represent constraints that must be satisfied by any more microscopic picture of catalysis by metal nanoparticles.

## ACKNOWLEDGMENTS

M.A.O. and R.F.L. acknowledge support from the National Science Foundation (NSF) through Grant No. CHE0743299. X.Z. and P.C. acknowledge support from the Army Research Office (USARO) (W911NF0910232), the National Science Foundation (NSF) (CBET-0851257), and the Department of Energy (DOE) (DE-FG02-10ER16199). We thank Weilin Xu for providing the data for 6 nm nanoparticles.

- <sup>1</sup>H. P. Lu, L. Xun, and X. S. Xie, *Science* **282**, 1877 (1998).
- <sup>2</sup>L. Edman, Z. Foldes-Papp, S. Wennmalm, and R. Rigler, *Chem. Phys.* **247**, 11 (1999).
- <sup>3</sup>L. Edman and R. Rigler, *Proc. Natl. Acad. Sci. U.S.A.* **97**, 8266 (2000).
- <sup>4</sup>S. L. Yang and J. S. Cao, *J. Phys. Chem. B* **105**, 6536 (2001).
- <sup>5</sup>S. L. Yang and J. S. Cao, *J. Chem. Phys.* **117**, 10996 (2002).
- <sup>6</sup>W. Min, B. P. English, G. B. Luo, B. J. Cherayil, S. C. Kou, and X. S. Xie, *Acc. Chem. Res.* **38**, 923 (2005).
- <sup>7</sup>S. C. Kou, B. J. Cherayil, W. Min, B. P. English, and X. S. Xie, *J. Phys. Chem. B* **109**, 19068 (2005).
- <sup>8</sup>B. P. English, W. Min, A. M. van Oijen, K. T. Lee, G. B. Luo, H. Y. Sun, B. J. Cherayil, S. C. Kou, and X. S. Xie, *Nat. Chem. Biol.* **2**, 87 (2006).
- <sup>9</sup>K. Velonia, O. Flomenbom, D. Loos, S. Masuo, M. Cotlet, Y. Engelborghs, J. Hofkens, A. E. Rowan, J. Klafter, R. J. M. Nolte, and F. C. de Schryver, *Angew. Chem. Int. Ed.* **44**, 560 (2005).
- <sup>10</sup>O. Flomenbom, K. Velonia, D. Loos, S. Masuo, M. Cotlet, Y. Engelborghs, J. Hofkens, A. E. Rowan, R. J. M. Nolte, M. Van der Auweraer, F. C. de Schryver, and J. Klafter, *Proc. Natl. Acad. Sci. U.S.A.* **102**, 2368 (2005).
- <sup>11</sup>O. Flomenbom, J. Klafter, and A. Szabo, *Biophys. J.* **88**, 3780 (2005).
- <sup>12</sup>O. Flomenbom and J. Klafter, *J. Chem. Phys.* **123**, 064903 (2005).
- <sup>13</sup>O. Flomenbom and R. J. Silbey, *Proc. Natl. Acad. Sci. U.S.A.* **103**, 10907 (2006).
- <sup>14</sup>O. Flomenbom, J. Hofkens, K. Velonia, F. C. de Schryver, A. E. Rowan, R. J. M. Nolte, J. Klafter, and R. J. Silbey, *Chem. Phys. Lett.* **432**, 371 (2006).
- <sup>15</sup>I. V. Gopich and A. Szabo, *J. Chem. Phys.* **124**, 154712 (2006).
- <sup>16</sup>W. Min, I. V. Gopich, B. P. English, S. C. Kou, X. S. Xie, and A. Szabo, *J. Phys. Chem. B* **110**, 20093 (2006).
- <sup>17</sup>G. De Cremer, M. B. J. Roeffaers, M. Baruah, M. Sliwa, B. F. Sels, J. Hofkens, and D. E. De Vos, *J. Am. Chem. Soc.* **129**, 15458 (2007).
- <sup>18</sup>J. A. Hanson, K. Duderstadt, L. P. Watkins, S. Bhattacharyya, J. Brokaw, J. W. Chu, and H. Yang, *Proc. Natl. Acad. Sci. U.S.A.* **104**, 18055 (2007).
- <sup>19</sup>B. C. Li, H. Yang, and T. Komatsuzaki, *Proc. Natl. Acad. Sci. U.S.A.* **105**, 536 (2008).
- <sup>20</sup>Y. W. Tan and H. Yang, *Phys. Chem. Chem. Phys.* **13**, 1709 (2011).
- <sup>21</sup>S. Kuznetsova, G. Zauner, T. J. Aartsma, H. Engelkamp, N. Hatzakis, A. E. Rowan, R. J. M. Nolte, P. C. M. Christianen, and G. W. Canters, *Proc. Natl. Acad. Sci. U.S.A.* **105**, 3250 (2008).
- <sup>22</sup>J. Cao, *J. Phys. Chem. B* **115**, 5493 (2011).
- <sup>23</sup>W. Xu, J. S. Kong, Y.-T. E. Yeh, and P. Chen, *Nature Mater.* **7**, 992 (2008).
- <sup>24</sup>W. Xu, H. Shen, G. Liu, and P. Chen, *Nano Res.* **2**, 911 (2009).
- <sup>25</sup>W. Xu, J. S. Kong, and P. Chen, *Phys. Chem. Chem. Phys.* **11**, 2767 (2009).
- <sup>26</sup>W. Xu, J. S. Kong, and P. Chen, *J. Phys. Chem. C* **113**, 2393 (2009).
- <sup>27</sup>P. Chen, W. Xu, X. Zhou, D. Panda, and A. Kalininskiy, *Chem. Phys. Lett.* **470**, 151 (2009).
- <sup>28</sup>X. Zhou, W. Xu, G. Liu, D. Panda, and P. Chen, *J. Am. Chem. Soc.* **132**, 138 (2010).
- <sup>29</sup>P. Chen, X. Zhou, H. Shen, N. M. Andoy, E. Choudhary, K.-S. Han, G. Liu, and W. Meng, *Chem. Soc. Rev.* **39**, 4560 (2010).
- <sup>30</sup>H. P. Lerch, A. S. Mikhailov, and B. Hess, *Proc. Natl. Acad. Sci. U.S.A.* **99**, 15410 (2002).
- <sup>31</sup>Z. Wu, V. Elgart, H. Qian, and J. Xing, *J. Phys. Chem. B* **113**, 12375 (2009).
- <sup>32</sup>R. Imbihl and G. Ertl, *Chem. Rev.* **95**, 697 (1995).
- <sup>33</sup>G. Ertl, *Faraday Discuss.* **121**, 1 (2002).
- <sup>34</sup>G. A. Somorjai and J. Y. Park, *Angew. Chem. Int. Ed.* **47**, 9212 (2008).
- <sup>35</sup>S. Wunder, Y. Lu, M. Albrecht, and M. Ballauff, *ACS Catal.* **1**, 908 (2011).
- <sup>36</sup>M. O. Vlad and J. Ross, *ChemPhysChem* **5**, 1671 (2004).
- <sup>37</sup>J. A. Hanson and H. Yang, *J. Chem. Phys.* **124**, 214101 (2008).
- <sup>38</sup>H. Yang, *J. Chem. Phys.* **129**, 074701 (2008).
- <sup>39</sup>B. C. Li, H. Yang, and T. Komatsuzaki, *J. Phys. Chem. B* **113**, 14732 (2009).

- <sup>40</sup>J. S. Cao, *Chem. Phys. Lett.* **327**, 38 (2000).
- <sup>41</sup>J. S. Cao, *Phys. Rev. E* **63**, 041101 (2001).
- <sup>42</sup>S. L. Yang and J. Cao, *J. Chem. Phys.* **121**, 572 (2004).
- <sup>43</sup>J. B. Witkoskie and J. S. Cao, *J. Chem. Phys.* **121**, 6361 (2004).
- <sup>44</sup>J. B. Witkoskie and J. S. Cao, *J. Chem. Phys.* **121**, 6373 (2004).
- <sup>45</sup>J. Cao, *J. Phys. Chem. B* **110**, 19040 (2006).
- <sup>46</sup>J. B. Witkoskie and J. Cao, *J. Phys. Chem. B* **110**, 19009 (2006).
- <sup>47</sup>J. B. Witkoskie and J. Cao, *J. Phys. Chem. B* **112**, 5988 (2008).
- <sup>48</sup>J. Cao and R. J. Silbey, *J. Phys. Chem. B* **112**, 12867 (2008).
- <sup>49</sup>I. V. Gopich and A. Szabo, *J. Chem. Phys.* **118**, 454 (2003).
- <sup>50</sup>M. O. Vlad, F. Moran, F. W. Schneider, and J. Ross, *Proc. Natl. Acad. Sci. U.S.A.* **99**, 12548 (2002).
- <sup>51</sup>M. O. Vlad, F. Moran, and J. Ross, *Chem. Phys.* **287**, 83 (2003).
- <sup>52</sup>H. Wang and H. Qian, *J. Math. Phys.* **48**, 013303 (2007).
- <sup>53</sup>Y. Zheng and F. L. H. Brown, *Phys. Rev. Lett.* **90**, 238305 (2003).
- <sup>54</sup>Y. Peng, Y. Zheng, and F. L. H. Brown, *J. Chem. Phys.* **126**, 104303 (2007).
- <sup>55</sup>Y. Peng, Y. Zheng, and F. L. H. Brown, *J. Chem. Phys.* **131**, 214107 (2009).
- <sup>56</sup>Y. He and E. Barkai, *J. Chem. Phys.* **122**, 184703 (2005).
- <sup>57</sup>D. S. Talaga, *J. Phys. Chem. A* **110**, 9743 (2006).
- <sup>58</sup>H. Qian and L. M. Bishop, *Int. J. Mol. Sci.* **11**, 3472 (2010).
- <sup>59</sup>R. Zwanzig, *Acc. Chem. Res.* **23**, 148 (1990).
- <sup>60</sup>R. Zwanzig, *J. Chem. Phys.* **97**, 3587 (1992).
- <sup>61</sup>T. Kuo, S. Garcia-Manyes, J. Li, I. Barel, H. Lu, B. J. Berne, M. Urbakh, J. Klafter, and J. M. Fernandez, *Proc. Natl. Acad. Sci. U.S.A.* **107**, 11336 (2010).
- <sup>62</sup>J. B. Witkoskie and J. S. Cao, *J. Chem. Phys.* **121**, 6361 (2004).
- <sup>63</sup>B. C. Stipe, M. A. Rezaei, and W. Ho, *J. Chem. Phys.* **107**, 6443 (1997).